Statistical Shape Analysis for Population Studies via Level-Set Based Shape Morphing⋆

Tammy Riklin Raviv, Yi Gao, James J. Levitt, and Sylvain Bouix

Psychiatry and Neuroimaging Laboratory, Brigram and Women Hospital,
Harvard Medical School

Abstract. We present a method that allows the detection, localization and quantification of statistically significant morphological differences in complex brain structures between populations. This is accomplished by a novel level-set framework for shape morphing and a *multi-shape* dissimilarity-measure derived by a modified version of the Hausdorff distance. The proposed method does not require explicit one-to-one point correspondences and is fast, robust and easy to implement regardless of the topological complexity of the anatomical surface under study.

The proposed model has been applied to different populations using a variety of brain structures including left and right striatum, caudate, amygdala-hippocampal complex and superior- temporal gyrus (STG) in normal controls and patients. The synthetic databases allow quantitative evaluations of the proposed algorithm while the results obtained for the real clinical data are in line with published findings on gray matter reduction in the tested cortical and sub-cortical structures in schizophrenia patients.

1 Introduction

The objective of the proposed study is the detection of morphometric differences in anatomical structures between different populations. We address this challenge via a novel and robust mathematical shape model equipped with a new parametrization-free shape metric. A variational framework, based on level-sets is the key concept in the proposed methodology avoiding some of the bottlenecks that are typical of numerous shape analysis applications – i.e. re-parametrization or calculation of one-to-one point correspondences. The suggested model allows to extract statistics that are sensitive enough to detect subtle changes between populations, yet robust enough to avoid common statistical errors.

Detection of shape changes in neurodevelopmental and or neurodegenerative diseases may shed new light on how illness impacts brain morphology. This hypothesis, and the recent advent of sophisticated computer algorithms, have led to many morphometric studies of brain anatomy in normal neurodevelopment.

There exist several general approaches to shape analysis. Perhaps the most common one is based on a surface representation of the objects, which are then

---

registered to each other to establish one-to-one correspondences [1–6]. This approach however involves difficult computational challenges, most notably establishing local correspondences within the population of objects and computing robust statistics. Medial representations (e.g. [7, 8]) while more compact, face similar challenges. Other methods represent a shape by a relatively small feature vector (e.g. [9, 10]). Such methods are usually numerically stable and allow for the computation of robust statistics. However, the resulting feature vectors are rarely intuitive making the interpretation of the results difficult.

In this paper we define a shape dissimilarity-measure, which is a generalization of the symmetrical Hausdorff distance between two objects (represented as binary maps). Let S_1 and S_2 be two distinctive point sets which may have a different cardinality, i.e. $|S_1| \neq |S_2|$. The classical definition of the Hausdorff distance $D_H(S_1, S_2)$ is as follows:

$$\max\{ \sup_{\mathbf{x}_1 \in S_1} \inf_{\mathbf{x}_2 \in S_2} d(\mathbf{x}_1, \mathbf{x}_2), \sup_{\mathbf{x}_2 \in S_2} \inf_{\mathbf{x}_1 \in S_1} d(\mathbf{x}_1, \mathbf{x}_2)\}, \tag{1}$$

where $d(x_1, x_2)$ is the Euclidean distance between points $x_1 \in S_1$ and $x_2 \in S_2$. When the maximum of the left and the right terms in Eq. (1) is replaced by their sum, this measure becomes symmetrical. In the proposed framework, we use a modified version of the symmetrical dissimilarity measure defined as follows:

$$D_m H(S_1, S_2) = \sum_{\mathbf{x}_1 \in S_1} \inf_{\mathbf{x}_2 \in S_2} d(\mathbf{x}_1, \mathbf{x}_2) + \sum_{\mathbf{x}_2 \in S_2} \inf_{\mathbf{x}_1 \in S_1} d(\mathbf{x}_1, \mathbf{x}_2), \tag{2}$$

which is more robust in the presence of noise and irregularities [11]. The minimum distance between a boundary voxel $\mathbf{x}$ in S_1 (or S_2) and the boundary voxels of the other shape S_2 (or S_1) is simply the value of the signed distance function (SDF) of S_2 (or S_1) in voxel $\mathbf{x}$. This connection allows us to represent shapes by signed distance functions (SDFs) or equivalently with level-sets [12]. The Hausdorff distance and the related Gromov-Hausdorff distance have been used before by e.g. [13–15] to define distances between point sets. For example in [13] the Gromov-Hausdorff distance was used for calculating the diffusion distance, rather than the geodesic path between points on a surface, allowing the comparison of pairs of non-rigid shapes with different topology. Here, the modified Hausdorff distance is used to define a level-set functional for the construction of the mean of a shape ensemble.

Our algorithm jointly constructs the mean of the given shape ensemble via a non-parametric shape deformation process derived by minimizing the proposed level-set functional and searches for the affine transformations that minimize the distances of the shapes to the evolved mean.

Spatial statistical analysis is obtained by calculating the minimal distance of each point on the mean shape surface to each of the affine registered input shapes. We then compute two-sample t-tests at every location on the mean shape surface to look for statistically significant differences between populations. The resulting raw p-values are adjusted for multiple comparison using the False Discovery Rate [16].

We test the proposed method on well-defined regions of interest using both synthetic and real data sets. The structures were selected for their importance with respect to brain regions implicated in schizophrenia and other neurological disorders. This includes synthetic sets of the striatum and the amygdala-hippocampal complex (AHC) and real data of the superior-temporal gyrus (STG) in first-episode schizophrenia patients and the caudate nucleus in women with schizotypal personality disorder (SPD) . We show that our algorithm can accurately detect, locate and quantify known morphological changes. Note that very few shape algorithms have been both qualitatively and quantitatively evaluated on ground truth data. Our results obtained for the clinical data are in line with previous findings of volumetric differences of the tested brain structures between schizophrenia patients and normal controls.

2   Methods

2.1   Shape Representation and Metric

A shape S_i is defined by the image region $\omega_i \subset \Omega$ that corresponds to the structure of interest, where $\Omega \in \mathbb{R}^3$ is the image domain. The boundary of ω_i is denoted by $\partial\omega_i$. Our representation of S_i is the signed distance function of its boundary: $\phi_{S_i} \colon \Omega \to \mathbb{R}$ such that the Eikonal equation $\|\nabla\phi_{S_i}\| = 1$ holds. We define the distance between S_i and S_j as the modified symmetrical Hausdorff distance between their boundaries using the continuous form of Eq. (2):

$$\mathbf{dist}(S_i, S_j) = \int_{\partial\omega_i} |\phi_{S_j}| d\mathbf{x} + \int_{\partial\omega_j} |\phi_{S_i}| d\mathbf{x} \tag{3}$$

As ϕ_{S_j} is a signed distance function, its absolute value in $\mathbf{x}$ represents the minimal Euclidean distance from $\mathbf{x}$ to the boundary of ω_j $(\partial\omega_j)$. The same applies for ϕ_{S_i} and $\partial\omega_i$. Formally, the signed distance of voxel $\mathbf{x} \in \partial\omega_i$ from ω_j is:

$$\mathbf{dist}(\mathbf{x} \in \partial\omega_i, S_j) = \phi_{S_j}(\mathbf{x}). \tag{4}$$

We define the mean S^M of a shape ensemble $\{S_1 \ldots S_N\}$, as the shape that minimizes the sum of the distances from all the shapes in the set:

$$\hat{S}^M = \arg\min_{S^M} \sum_{i=1}^{N} \mathbf{dist}(S_i \circ \hat{T}_{i,M}, S^M), \tag{5}$$

where $\hat{T}_{i,M}$ is the estimated affine trasformation that aligns a shape S_i to the mean shape as will be described next.

2.2   Alignment of Shapes

As in [17], we define 'shape' as a set of geometric features of an object that is invariant to 12-parameter affine transformation. It is thus necessary to remove the affine components differentiating the input objects before computing statistics over populations. We use a group-wise registration framework in which each

shape S_i is registered by an affine transform to the estimated mean shape $\hat{S}^M$ such that the modified Hausdorff distance, defined in Eq. 3 is minimized:

$$\hat{T}_{i,M} = \arg \min_{T_{i,M}} \mathbf{dist}(S_i \circ T_{i,M}, \hat{S}^M). \tag{6}$$

2.3   Joint Group-Wise Registration and Mean Shape Evolution

As neither the mean shape S^M nor the affine parameters $T_{i,M}$ that aligns each shape S_i to the mean are known, we use an alternating minimization technique in which Eq. (6) (for each shape S_i in the ensemble) and Eq. (5) are jointly solved. While the affine transformation parameters are inferred by using a global optimization method [18] the mean shape is generated via gradient descent optimization of a level-set functional. The signed distance functions $\{\phi_{S_i}\}$ can be viewed as level-set functions, where their zero levels define the boundaries of the respective shapes. In the spirit of [19] we use the sigmoidal "logistic" function of ϕ as a regularized form of the Heaviside function :

$$H_\epsilon(\phi) = \frac{1}{2}\left(1 + \tanh\left(\frac{\phi}{2\epsilon}\right)\right) = \frac{1}{1 + e^{-\phi/\epsilon}}, \tag{7}$$

The boundary of a shape S_i can be therefore approximated by $\partial \omega_{S_i} = |\nabla H_\epsilon(\phi_{S_i})|$ defining the distance between S^M and the shape set $\{S_i\}$ as follows [1]:

$$D(S^M, \{S_i\}) = \sum_i \int_\Omega [|\phi_{S^M}||\nabla H_\epsilon(\phi_{S_i})| + |\phi_{S_i}||\nabla H_\epsilon(\phi_{S^M})|]\, d\mathbf{x}. \tag{8}$$

We estimate ϕ_{S^M} iteratively:

$$\hat{\phi}_{S^M} = \arg \min_{\phi_{S_M}} D(S^M, \{S_i\}). \tag{9}$$

The gradient descent equation that determines the evolution of ϕ_{S^M} is derived from the first variation of the functional in equation (8):

$$\phi_t^M = \sum_i \left[\mathrm{sign}(\phi_{S^M})|\nabla H_\epsilon(\phi_{S_i})| + \delta_\epsilon(\phi_{S^M})\mathrm{div}\left(\frac{\nabla \phi_{S^M}}{|\nabla \phi_{S^M}|}|\phi_{S_i}|\right)\right], \tag{10}$$

where $\mathrm{sign}(\cdot)$ is the sign function; $\mathbf{div}$ is the divergence operator and $\delta_\epsilon(\phi)$ is the derivative of $H_\epsilon(\phi)$ with respect to ϕ.

2.4   Implementation

The ensemble shapes are first aligned by translation such that the center of mass of each shape coincides with the mean of the centers of mass of all the shapes. We then average the shape, defining an 'approximate' mean and calculate the

---

[1] Hereafter, $S_i \circ T_{M,i}$ is represented as S_i to simplify the notation.

affine transformations of each shape to that mean. Then a better approximation to the mean shape is calculated by averaging the affine-transformed shapes. We use the approximated mean shape to initialize the level-set-based gradient descent process.

Averaging over the set of SDFs, i.e. $\phi_1, \ldots, \phi_N$, will not result in a valid SDF representation as the mean of SDFs is not an SDF. We instead use the logistic functions of the SDFs as in Eq. (7) folowing [20]. In practice, we average the regularized Heaviside functions of the SDFs, i.e. $H(\phi_i)$. The boundary of the mean shape, $\partial \omega_{\text{Mean}}$, is the 0.5 level set of the mean probability map. The underlying assumption here is that the morphological variability of an anatomical structure within different subjects, even across populations, is sufficiently small such that the high-dimensional points that represent the shape ensemble lie in close proximity to each other upon the shape manifold. Therefore their mean (used for initialization) is approximately on the manifold, as well.

2.5   Localization of Shape Differences between Populations

We now present how our model can effectively detect local shape deformations within a population. Given a point on the mean shape boundary, $\mathbf{x} \in \partial \omega_{\text{Mean}}$, we can directly obtain its signed distance to each of the affine aligned shapes, by looking up the distance in the corresponding SDF $\phi_n(\mathbf{x})$. For each of those voxels, statistics on the $\phi_n(\mathbf{x})$ can capture local thickening or thinning of structure as well as more complex boundary displacements not removed by the affine transformation.

Let $\phi_1^*, \ldots, \phi_N^*$ and $\phi_1^{**}, \ldots, \phi_M^{**}$ be the signed distance functions representing shapes of a particular anatomical structure in two populations. Let $d^*(\mathbf{x})$ and $d^{**}(\mathbf{x})$ be two vectors of lengths N and M respectively of the (signed) distances of the corresponding shape ensembles to $\mathbf{x}$. We can now apply two-sample t-tests (or another statistic) at each location on the boundary to look for statistically significant differences between the two populations. In the following experiments, we also use False Discovery Rate (FDR) to correct for multiple comparisons [16].

3   Experiments

We evaluated the proposed algorithm using synthetic and real data sets: synthetic sets of the amygdala-hippocampal complex (AHC) and of the striatum, and real data of the superior-temporal gyrus (STG) in first episode schizophrenics and the caudate nucleus in women with schizotypal personality disorder (SPD) . All results were corrected for multiple comparisons using the FDR approach in [16]. We applied a false discovery rate of 5%.

3.1   Synthetic Amygdala-Hippocampal Complex

Manual segmentations of the left amygdala-hippocampus complexes (AHC) in 40 normal controls were taken from the laboratory database. An unbiased atlas

of the AHC was created from the 40 samples [21]. The resulting atlas was then warped back to subject space using 20 randomly selected inverse warps obtained in the previous step. The resulting samples compose the normal control group (NC). The remaining 20 were manipulated by adding (or removing) a specific number of voxels using a hemisphere such that either a bump (or dimple) would be created and labeled "abnormal" (AB). Eight pairs of NC/AB data sets were generated. Each AB set had a bump (or a dimple) located in the head of the AHC and with a radius of $3, 4, 5$ and 6 voxels respectively.

For each AB/NC data set, we generated the mean AHC and performed a t-test comparing the NC and AB distances to the mean at each point on the mean shape's surface. Successful results of these eight experiments ({bump,dimple} $\times \{3, 4, 5, 6\}$) are shown in Fig. 1. We also evaluated the method by looking at the ratio of the statistically significant voxels over the total number of surface voxels for the bump (dimple) as the size of the deformation increases (Fig. 2).

$r = 3$ Vox. $r = 4$ Vox. $r = 5$ Vox. $r = 6$ Vox.
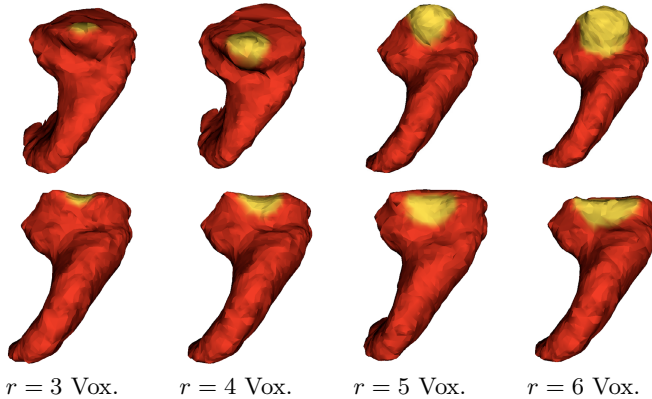
Fig. 1. AHC data set. p-value maps displayed on the mean shapes of NC/AB data sets with a bump (top row) or dimple (bottom row) of radius (from left to right) $3, 4, 5$ and 6. Red indicates non-significant p-values while the yellow colors present a scale of FDR corrected p-values (below the threshold).
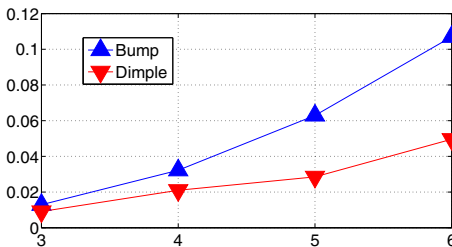
Fig. 2. Method evaluation for the synthetic AHC datasets. The ratio of the statistically significant mean shape surface voxels over the total number of surface voxels increases as the size of the synthetic distortion (bump or dimple) increases.

3.2   Synthetic Striatum

Synthetic striatum shapes were generated through manifold learning based on a training set of 27 real samples [22]. Abnormal examples were generated via random processes of either thinning or thickening of specific, well define regions of the striatum (see Fig. 3a-c,e-g). Two sets of examples for the right and the left striatum, each containing 50 normal and 50 abnormal examples, were tested. Results are shown in Fig. 3. Note that the distorted regions (highlighted in red) - corresponding to voxels with significant (FDR corrected) p-values (Fig. 3 d,h) were precisely detected.

a   b   c   d

e   f   g   h
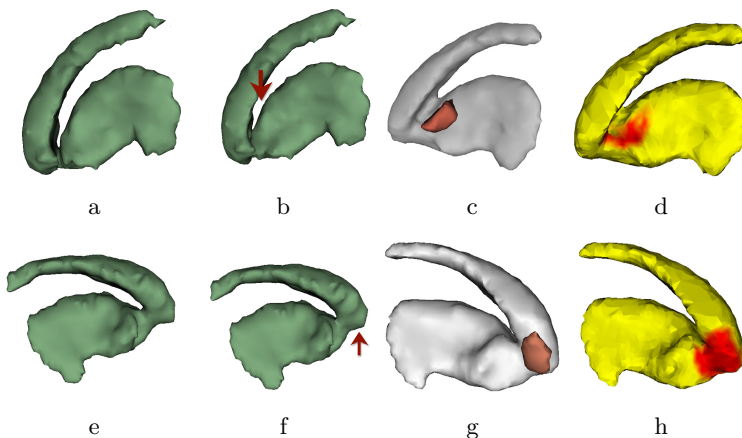
Fig. 3. Left (top) and Right (bottom) Striatum data sets. (a,e) Randomly selected examples of the left (a) and the right (e) striatum. (b,f) Left (b) and right (f) striatum shapes after applying shape deformations to the respective shapes shown in (a,e). (c,g) Mean (left and right) striatum shapes along with the averaged artificial deformation (red) (d,h) Mean (left and right) striatum shapes along with the respective p-value maps comparing distorted and undistorted data sets. Yellow indicates non-significant p-values. Red colors present a scale of FDR corrected p-values (below the threshold). Note that although the deformations and the extent of the deformed regions (pointed by arrows) are subtle, they were successfully detected by our algorithm.

3.3   STG in First Episode Schizophrenic Patients

We used manual segmentation of the left and right STGs in 19 patients diagnosed with first episode schizophrenia and 14 matched normal controls originally acquired for a brain volumetric study [23]. Examples of the left STG of some of the subjects are shown in Fig. 4.

We generated the mean shapes of the patients and NC data sets for the left and right STG. We computed a t-test comparing the two populations at each point on the mean shape's surface. The resulting p-values were thresholded at an

FDR of 0.05. Qualitative results are shown in Figs. 5. We were able to detect and locate morphological differences between populations in the left STG. Moreover, most of the shape differences in the STG were detected in the planum temporale (Fig. 5a, in red) and the heschl gyrus (Fig. 5a, in green). These findings are in line with the recent literature on volumetric studies in schizophrenia [24].

a   b   c   d   e
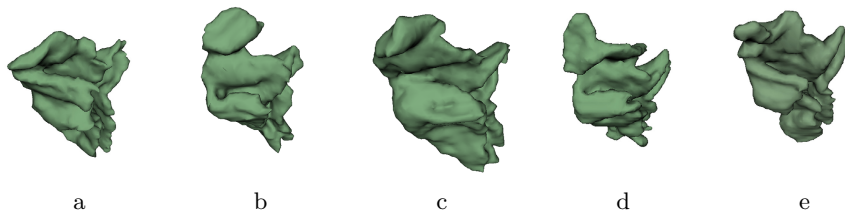
Fig. 4. Left STG of first episode schizophrenics. A few examples demonstrating the complexity of this structure and its variability among patients.

a   b   c
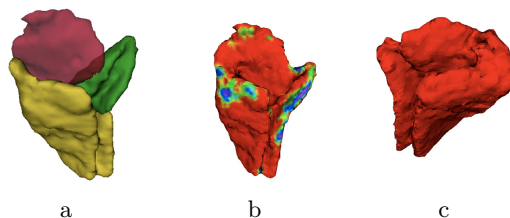
Fig. 5. STG in first episode schizophrenia. (a) Left STG composed of its substructures: planum temporale (red), heschl's gyrus (green), rest of the STG (yellow); (b) p-value map of the left STG comparing schizophrenics and NCs; (c) p-value map of the right STG Left for the same populations. Red indicates non-significant p-values, green-to-purple colors present a scale of p-vales below the 0.05 FDR threshold. Note that the right STG shows no differences.

3.4   Caudate Nucleus in Schizotypal Personality Disorder (SPD) Patients

MR brain scans of 61 women, 32 SPD patients and 29 NC, were manually segmented to extract the caudate nucleus in the left and right hemispheres [25] . Statistically significant morphological differences have been detected in the right caudate using the proposed algorithm (Fig. 6). Our results in these subjects are comparable to the manual volumetric measures as well as to the shape statistics obtained from using spherical harmonic-point distribution model (SPHARM-PDM) methodology [25].

a   b   c   d
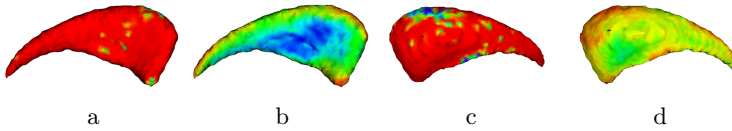
Fig. 6. Caudate nucleus in SPD patients. (a,c) Lateral and medial views of the mean right caudate along with the respective p-value maps. Red indicates non-significant p-values. Yellow-to-blue indicate p-value below a 0.05 FDR. (b,d) Signed differences between the SPD patients and the NC. Negative values (deflation) are in red, positive values (inflation) in dark blue.

4   Discussion

We presented a robust and simple framework to perform shape analysis for population studies. The core of the method is a novel-level set algorithm based on the modified Hausdorff distance for shape morphing.

Our experiments on synthetic data show the ability of the method to detect small deformations of complex shapes such as the striatum. Very few boundary based methods are able to address such convoluted shapes and, as far as we know, have not been tested thoroughly on synthetic data. In addition, we were able to find shape differences between patients and their controls in the left STG and the right caudate which are consistent with the prior finding based on manual segmentation. Finally, while we acknowledge that the geodesics upon the shape ensemble manifolds are only roughly approximated by the modified Hausdorff distances our experiments show that in practice they can be used as accurate and reliable measures to perform population studies.

References

1. Cates, J.E., Fletcher, P.T., Styner, M.A., Hazlett, H.C., Whitaker, R.T.: Particle-Based Shape Analysis of Multi-object Complexes. In: Metaxas, D., Axel, L., Fichtinger, G., Székely, G. (eds.) MICCAI 2008, Part I. LNCS, vol. 5241, pp. 477–485. Springer, Heidelberg (2008)
2. Chen, T., Vemuri, B., Rangarajan, A., Eisenschenk, S.: Group-wise point-set registration using a novel cdf-based havrda-charvt divergence. International Journal of Computer Vision 86, 111–124 (2010)
3. Kurtek, S., Klassen, E., Ding, Z., Jacobson, S., Jacobson, J., Avison, M., Srivastava, A.: Parameterization-invariant shape comparisons of anatomical surfaces. IEEE Trans. Med. Imaging 30, 849–858 (2011)
4. Shen, L., Farid, H., McPeek, M.A.: Modeling 3-dimensional morphological structures using spherical harmonics. Evolution 63, 1003–1016 (2009)
5. Styner, M., Lieberman, J., Pantazis, D., Gerig, G.: Boundary and medial shape analysis of the hippocampus in schizophrenia. Medical Image Analysis, 197–203 (2004)
6. Thompson, P., et al.: Mapping hippocampal and ventricular change in alzheimer disease. NeuroImage 22, 1754–1766 (2004)

7. Styner, M., et al.: Statistical shape analysis of neuroanatomical structures based on medial models. Medical Image Analysis 7, 207–220 (2003)
8. Yushkevich, P.A., Zhang, H., Gee, J.C.: Continuous medial representation for anatomical structures. Medical Image Analysis 25, 1547–1564 (2006)
9. Mangin, J., et al.: Brain morphometry using 3D moment invariants. Medical Image Analysis 8, 187–196 (2004)
10. Niethammer, M., Reuter, M., Wolter, F.-E., Bouix, S., Peinecke, N., Koo, M.-S., Shenton, M.E.: Global Medical Shape Analysis Using the Laplace-Beltrami Spectrum. In: Ayache, N., Ourselin, S., Maeder, A. (eds.) MICCAI 2007, Part I. LNCS, vol. 4791, pp. 850–857. Springer, Heidelberg (2007)
11. Dubuisson, M., Jain, A.: A modified hausdorff distance for object matching. In: ICPR, vol. 1, pp. 566–568 (1994)
12. Osher, S., Sethian, J.A.: Fronts propagating with curvature-dependent speed: Algorithms based on Hamilton-Jacobi formulations. Journal of Computational Physics 79, 12–49 (1988)
13. Bronstein, A.M., Bronstein, M.M., Kimmel, R., Mahmoudi, M., Sapiro, G.: A gromov-hausdorff framework with diffusion geometry for topologically-robust non-rigid shape matching. International Journal of Computer Vision 89, 266–286 (2010)
14. Charpiat, G., Faugeras, O., Keriven, R., Maurel, P.: Statistics and Analysis of Shapes: Approximations of Shape Metrics and Application to Shape Warping and Empirical Shape Statistics. Krim, H., Yezzi Jr., A. (eds.) (2006)
15. Memoli, F., Sapiro, G.: A theoretical and computational framework for isometry invariant recognition of point cloud data. Foundations of Computational Mathematics 5, 313–347 (2005)
16. Nichols, T., Hayasaka, S.: Controlling the familywise error rate in functional neuroimaging: A comparative review. Stat. Meth. Med. Research 12, 419–446 (2003)
17. Ashburner, J., Friston, K.J.: Voxel-based morphometry – the methods. NeuroImage 11, 805–821 (2000)
18. Jenkinson, M., Smith, S.: A global optimisation method for robust affine registration of brain images. Medical Image Analysis 5, 143–156 (2001)
19. Chan, T., Vese, L.: Active contours without edges. IEEE Transactions on Image Processing 10, 266–277 (2001)
20. Pohl, K., et al.: Using the logarithm of odds to define a vector space on probabilistic atlases. Medical Image Analysis 11, 465–477 (2007)
21. Sabuncu, M.R., Yeo, B.T.T., Van Leemput, K., Vercauteren, T., Golland, P.: Asymmetric Image-Template Registration. In: Yang, G.-Z., Hawkes, D., Rueckert, D., Noble, A., Taylor, C. (eds.) MICCAI 2009, Part I. LNCS, vol. 5761, pp. 565–573. Springer, Heidelberg (2009)
22. Gao, Y., Bouix, S.: Synthesis of realistic subcortical anatomy with known surface deformations. In: MICCAI Workshop on Mesh Processing in Medical Image Analysis (October 2012)
23. Hirayasu, Y., et al.: Lower left temporal lobe MRI volumes in patients with first-episode schizophrenia compared with psychotic patients with first-episode affective disorder and normal subjects. Amer. J. Psychiatry 155, 1384–1391 (1998)
24. Shenton, et al.: A review of MRI findings in schizophrenia. Schizophrenia Research 49, 1–52 (2001)
25. Levitt, et al.: Shape abnormalities of caudate nucleus in schizotypal personality disorder. Schizophr Res. 110, 127–139 (2009)